Optical Engineering

SPIEDigitalLibrary.org/oe

$Al/SiO_x/Al$ single and multiband metamaterial absorbers for terahertz sensor applications

Brian Kearney
Fabio Alves
Dragoslav Grbovic
Gamani Karunasiri

SPIE

Al/SiO_x/Al single and multiband metamaterial absorbers for terahertz sensor applications

Brian Kearney
Fabio Alves
Dragoslav Grbovic
Gamani Karunasiri
Naval Postgraduate School
Building 232, Room 204B
833 Dyer Road
Monterey, California 93943
E-mail: karunasiri@nps.edu

Abstract. To increase the sensitivity of uncooled thermal sensors in the terahertz (THz) spectral range (1 to 10 THz), we investigated thin metamaterial layers exhibiting resonant absorption in this region. These metamaterial films are comprised of periodic arrays of aluminum (Al) squares and an Al ground plane separated by a thin silicon-rich silicon oxide (SiO_x) dielectric film. These standard MEMS materials are also suitable for fabrication of bi-material and microbolometer thermal sensors. Using SiO_x instead of SiO_2 reduced the residual stress of the metamaterial film. Finite element simulations were performed to establish the design criteria for very thin films with high absorption and spectral tunability. Single-band structures with varying SiO_x thicknesses, square size, and periodicity were fabricated and found to absorb nearly 100% at the designed frequencies between three and eight THz. Multiband absorbing structures were fabricated with two or three distinct peaks or a single-broad absorption band. Experimental results indicate that is possible to design very efficient thin THz absorbing films to match specific applications. [DOI: 10.1117/1.OE.52.1.013801]

Subject terms: terahertz; metamaterial; perfect absorber; thermal sensor.

Paper 121289P received Sep. 6, 2012; revised manuscript received Nov. 30, 2012; accepted for publication Dec. 4, 2012; published online Jan. 18, 2013.

1 Introduction

Imaging with terahertz (THz) radiation is attractive for security[1] and medical[2,3] applications due to its ability to penetrate most dry, nonmetallic, nonpolar materials without damaging them, while resolving details such as skin features and metallic objects.[1–5] Unfortunately, background THz emission at 300 K is minute compared to shorter wavelength infrared (IR) radiation, and uncooled imaging in this spectral range is done either in transmission or reflection mode using a THz illuminating source.[1–3,6–8] Uncooled microbolometers optimized for 8 to 12-μm IR radiation coupled with THz quantum cascade lasers (QCLs) have been shown to be an effective imaging system.[6–8] Uncooled IR microbolometers generally have a noise equivalent power (NEP) in the THz range of approximately 300 $pW/Hz^{1/2}$ in Ref. 9 compared to a NEP of 14 $pW/Hz^{1/2}$ for the IR range[10] implying low responsivity at THz frequencies. This reduced responsivity is primarily due to poor absorption of THz radiation by the pixel membrane, which is primarily made of Si_3N_4.[9] The ability of metamaterials to exhibit optical properties not found in their constituents makes them attractive absorbers because their optical properties can be tailored through the geometry of their subwavelength features, while the properties of the constituent materials remain unchanged. With the proper geometry, a 'perfect' absorber can be constructed for specific frequencies.[11] One option for enhancing the THz absorption of thermal sensors is to integrate a thin metamaterial film tuned to the illuminator frequency.[12,13] We have previously fabricated single-band absorbers[12] and have successfully integrated them onto bi-material THz sensors.[13] Integration of IR meta-materials onto microbolometers[14] and subterahertz split-ring resonators onto bi-material sensors[15] for improving absorption have also been performed by others. These metamaterial films typically consist of a periodic-patterned metal layer, a dielectric spacer, and a ground plane.[12–14,16–25] Multiband absorbers have also been demonstrated in GHz,[17–19] 0.1 to 1 THz,[20,21] 1 to 10 THz,[22–24] and IR[25,26] ranges. However, the multiband absorbers in the 1 to 10 THz range rely on 8-μm[22] and 4-μm[23,24] thick layers of polyimide as the dielectric spacer layer. Since microbolometer pixel membranes are typically about 0.5-μm thick,[11] the use of 4- to 8-μm films would substantially increase thermal capacitance, negatively impacting real-time imaging performance due to an increase in the thermal time constant. Therefore, we explore the use of thin layers of low stress silicon-rich silicon oxide (SiO_x) as the dielectric, which can also be incorporated into microbolometer and bi-material based THz sensors.[13] Sensors integrating these high THz-absorbing layers will have smaller thermal time constants and thus an improved speed of operation compared to other thicker metamaterial absorbers in this spectral range. Low stress silicon-rich silicon oxide (SiO_x) was chosen as the dielectric spacer to reduce the intrinsic stress of microcantilevers compared to stoichiometric SiO_2 used in Ref. 13. In this paper, we present experimental results for THz absorbing metamaterial films with single- and multiple-absorption peaks.

2 Design and Modeling

Figure 1 shows the basic configuration (unit cell) that we employed, which involves a ground plane of metal, a dielectric spacer, and an additional metal layer patterned into an array of squares. It should be noted that the wavelength range for 3 to 8 THz radiation in SiO_x is approximately 19 to 53 μm, more than 10 times the thickness of these

0091-3286/2013/$25.00

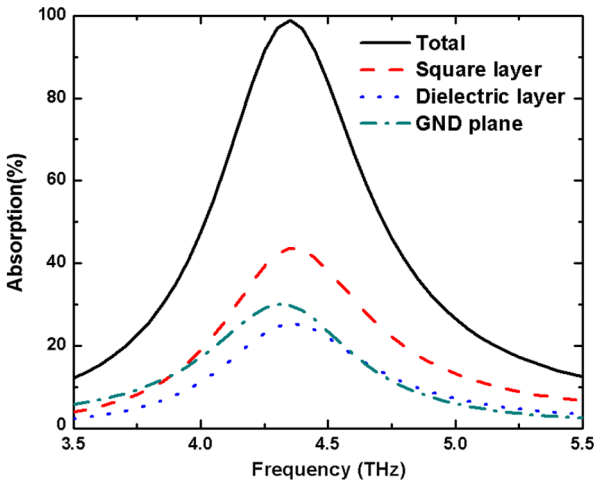

Fig. 1 Modeled absorption characteristics of the three layers of a metamaterial with single absorption peak.

absorbing layers. When incident electromagnetic (EM) radiation strikes the metamaterial layer, it induces localized surface plasmon resonances.[12,14] Resistive losses in the metal and dielectric layers convert some of the incident energy to heat, allowing the radiation to be absorbed. Resonant absorption frequency (ν) and absorption magnitude can be understood using explanations such as impedance-matching to free space,[27] an equivalent resistor inductor capacitor (RLC) circuit,[12,14] confined TM cavity modes,[16] interference of multiple reflections,[28] and transmission lines.[29] The relatively complex nature of metamaterial structures makes numerical simulations generally the preferred modeling method.

Finite element (FE) analysis, performed with COMSOL multiphysics software, was used to model the absorption characteristics of the metamaterial absorbers. The COMSOL RF module can allow penetration of an incident plane wave of THz radiation with a particular intensity and propagation direction into a surface using scattering boundary conditions or a plane wave generation on a boundary using internal ports [Fig. 2(b)]. The periodic nature of these absorbing films allows the model to be simplified to a unit cell, complete with periodic boundary conditions. A unit cell for a single-band absorber is shown in Fig. 2(a), with all domains, other than metal or dielectric, assumed to be free space. Perfect electric conductors (PEC) and perfect magnetic conductors (PMC) were used as periodic boundary conditions for normally incident radiation while Floquet boundary conditions were used for simulations involving incoming THz radiation at oblique incidence. As the difference in magnitude between the absorption peaks of normal and near-normal incident is only a few percent and the absorption frequency is essentially unchanged, PEC and PMC boundary conditions are generally preferable in most situations to reduce computation time as in Ref. 12.

When using internal ports, the magnitude and direction of the Poynting vector are known in the model, one can retrieve reflection and transmission coefficients by integrating the Poynting vector along boundaries below the metamaterial layer and above the internal port, respectively, or the losses in the respective PML layers above these boundaries.[12] Alternatively, to save additional computation time, scattering boundary conditions can be used and the absorption can be retrieved directly by integrating the resistive losses (and magnetic, when applicable) in the material. As all the constitutive relations used in these models are assumed to be linear, it is convenient to set the radiation flux into the unit cell to 1 W, allowing the total resistive losses to simply be read off as the absorption coefficient. Results from this method can be compared and validated by retrieving the reflection and transmission coefficients directly. An additional advantage of integrating resistive losses is that the contribution of individual layers can be examined separately, where reflection and transmission coefficients only reveal the total power absorbed. Figure 2(c) shows the average power flux (arrows) in the structure of Fig. 2(a). No observable power flux is seen below the metamaterial layer because the ground plane is thicker than the skin depth of Al (approximately 80 nm at 4 THz). Figure 1 shows modeled spectral characteristics of the absorption of different layers for the

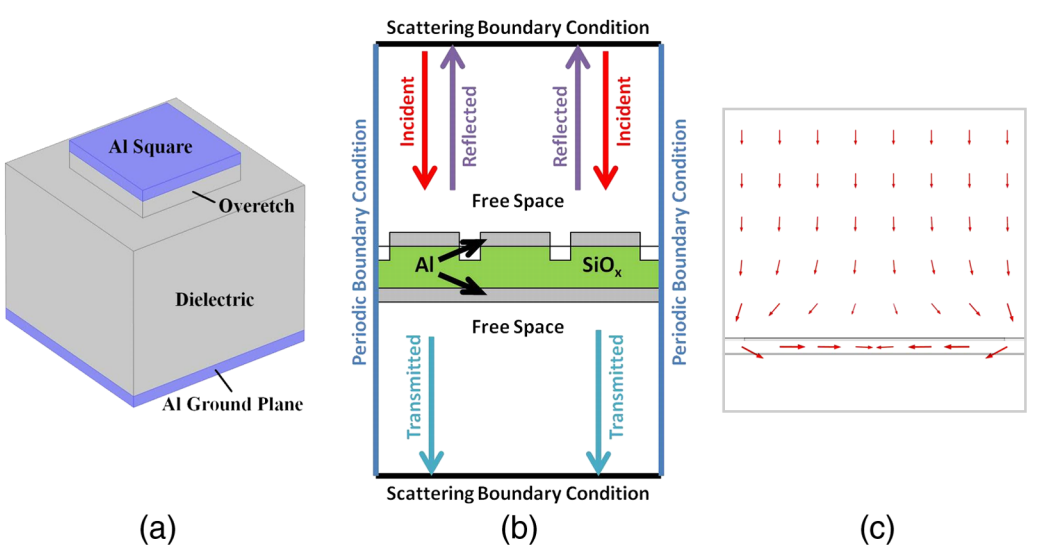

Fig. 2 Unit cell (a) of a metamaterial with a single absorption peak. The model also incorporates the unintentional over-etch into the SiO$_x$ during the fabrication. Schematic representation (b) of the unit cell in the FE modeling program with boundary conditions and THz plane wave at normal incidence. Time-averaged power flow (c) near the resonant absorption frequency and arrow lengths relate to magnitude in log scale.

structure in Fig. 2(a) with a square size of 16 μm, SiO_2 thickness of 1.2 μm, square pitch of 21 μm, and no overetching. It can be seen that the amount of absorption varies from layer to layer, even if the layers are constructed of the same material.

This is expected as EM fields can vary due to the spatial location of these layers. However, the losses in a particular layer are important if this layer is to be thermally isolated from others in a thermal sensor. An additional advantage of FE modeling of metamaterials is that the experimental absorption data can be used to obtain the optical properties of the constituent materials.

3 Fabrication and Measurement

The metamaterial absorbing layers, comprised of a patterned metal film (Al) consisting of different configurations of subwavelength squares separated by a dielectric layer (SiO_x) from a metallic ground plane (Al), were fabricated using standard microfabrication techniques.[12] The first step involved depositing 90 nm of Al on 4-in. Si substrates using e-beam evaporation. Next, low stress SiO_x layers of various thicknesses were deposited with plasma enhanced chemical vapor deposition (PECVD). These nonstochiometric SiO_x layers contain more Si than standard stochiometric SiO_2 depositions, reducing residual stress for a 350°C deposition to approximately −13 from −140 MPa for SiO_2. Incorporating SiO_x may help alleviate the excessive residual stress-related deformation observed in the sensors fabricated in Ref. 13. Thicknesses of the SiO_x layers were determined using optical interferometrics to be: 0.359, 0.546, 0.738, 0.919, 1.115, 1.283, 1.470, and 1.662 μm. Following oxide deposition, e-beam evaporation was used to deposit an additional 90 nm of Al over the SiO_x. This layer was patterned using contact photolithography followed by Ar sputter-etching. The conductivity of the aluminum layers was determined to be about 1×10^7 S/m using a four-point probe. Twenty five separate sectors on each wafer were patterned with metamaterials with varying square size and pitch, as shown by an optical image of one of the fabricated wafers in Fig. 3. Stylus profilometer measurements indicated an unintentional overetching of the Al layer into the SiO_x layer of approximately 150 nm in every wafer. Square dimensions and pitch were measured using optical microscopy. Wafers with the same metamaterial designs, but different dielectric thicknesses, were also fabricated to explore the effects of dielectric layer thickness on the absorption. The absorption characteristics for different square sizes and dielectric thicknesses were examined and compared to that of simulations as described in the following sections.

The ground plane of Al prevents any significant transmission of THz radiation, allowing $A + T + R = 1$ to be simplified to $A \approx 1 - R$. Unpolarized reflectance (R) measurements were performed at 15 deg-incidence using a Thermo-Nicolet Nexus 870 Fourier Transform Infrared Spectrometer (FTIR) with a globar source fitted with a PIKE Technologies MappIR accessory. A gold-coated Si wafer was used to establish the background for the reflectance measurements.

For example, simulation of a unit cell of one of the structures with 21-μm period and 16-μm Al squares, using the measured conductivity of Al of 1×10^7 S/m and a complex index of refraction for SiO_2 at 2 THz of 2 to 0.025i from,[30] is compared to an FTIR measurement in Fig. 4. The slight difference between the simulation and measurement can be attributed to the use of SiO_2 parameters to represent SiO_x layer.

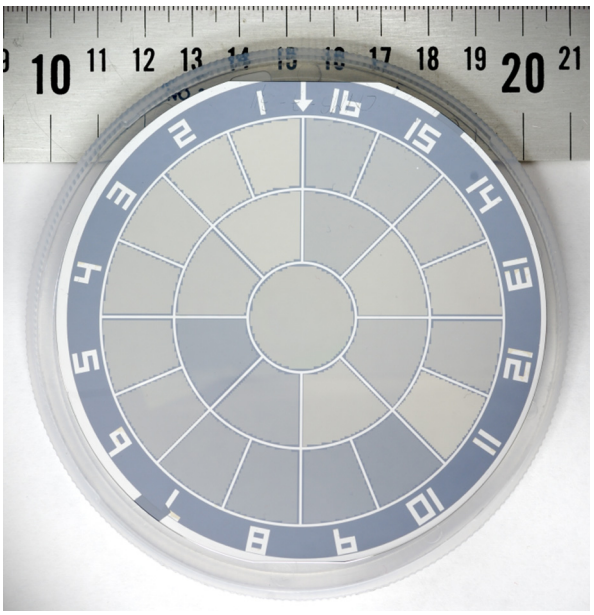

Fig. 3 One of the fabricated wafers with 25 different metamaterials arranged radially for automated reflection measurement using a PIKE MappIR FTIR accessory.

4 Metamaterials with a Single Absorption Peak

The metamaterials with a single absorption peak were fabricated with variations in square size, pitch, and dielectric layer thickness. Periodic structures with 21 μm pitch were fabricated with Al square sizes from 9 to 18 μm with 1 μm increments to determine the effect of square dimension on the resonant frequency and absorption strength. Additionally, each wafer also contains metamaterial structures having 16 μm squares with pitch varying from 19 to 25 μm with 1 μm increments to probe the effect of pitch on the absorption spectrum. Figure 5(a) shows the measured absorption spectra as a function of the square dimension, which indicates that as the square size increases the peak

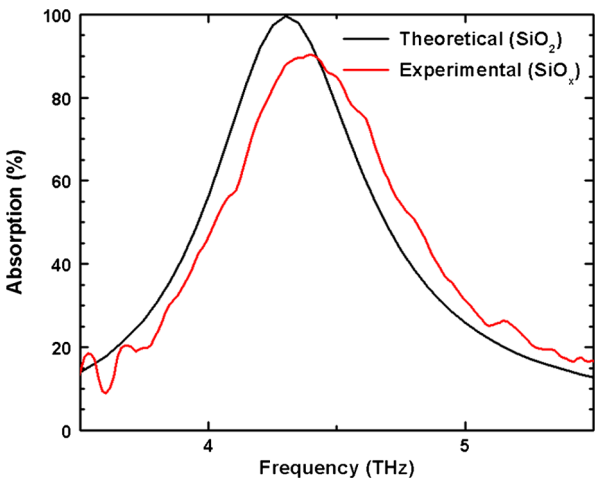

Fig. 4 Comparison of the experimental data with FE model using SiO_2 material parameters at 2 THz.

absorption frequency decreases. The plot in Fig. 5(b) shows that the peak frequency is inversely proportional to the square size. This behavior is anticipated as the wavelength of the confined modes should correspond to the current distributions and E-fields observed in FE simulations. The lowest order mode consists of a single oscillating dipole formed by the incident radiation interacting with the square with opposing currents and charges in the ground plane, and thus the wavelength of any trapped first-order modes should be proportional to the size of the structure in the direction of the incident E-field component parallel to the surface.

Figure 5(c) shows the absorption spectra for a set of dielectric layer thicknesses where the square dimension and pitch remained constant. It can be seen in Fig. 5(c) that the shift of resonant frequency due to dielectric layer thickness is relatively small, while the strength of absorption is significantly enhanced as the dielectric layer thickness increases. In the case of these 12 μm squares, the highest absorption was achieved with a dielectric layer thickness of 1.66 μm. Absorption models predict a reduction in absorption amplitude when the dielectric layer is thicker than the optimal value.[16,28,29] No reduction in absorption amplitude was observed for increased thickness in this range, suggesting that all absorbers described have an optimal thickness at or above 1.66 μm. It is important to keep the dielectric layer as thin as possible when using metamaterials for thermal sensor applications to reduce thermal capacitance, and thus increase the detector's speed of operation.

Furthermore, the dependence of spectral characteristics of metamaterials on the pitch of the square array was probed by keeping the rest of the parameters constant. Intuitively, one would expect the absorption of thin metamaterials to increase with a smaller pitch due to a higher density of squares[12,14] or better coupling to external radiation.[16] Decreasing the pitch does improve the maximum absorption for 16 μm squares [Fig. 5(d)]. A small change in resonant frequency is also apparent. However, a minor reduction in square size could easily offset this shift. Clearly, this should simultaneously reduce coupling between squares due to larger gaps between squares, increasing resonant frequency further.

The measurements show that single-band resonant absorbers can be designed with nearly 100% absorption in

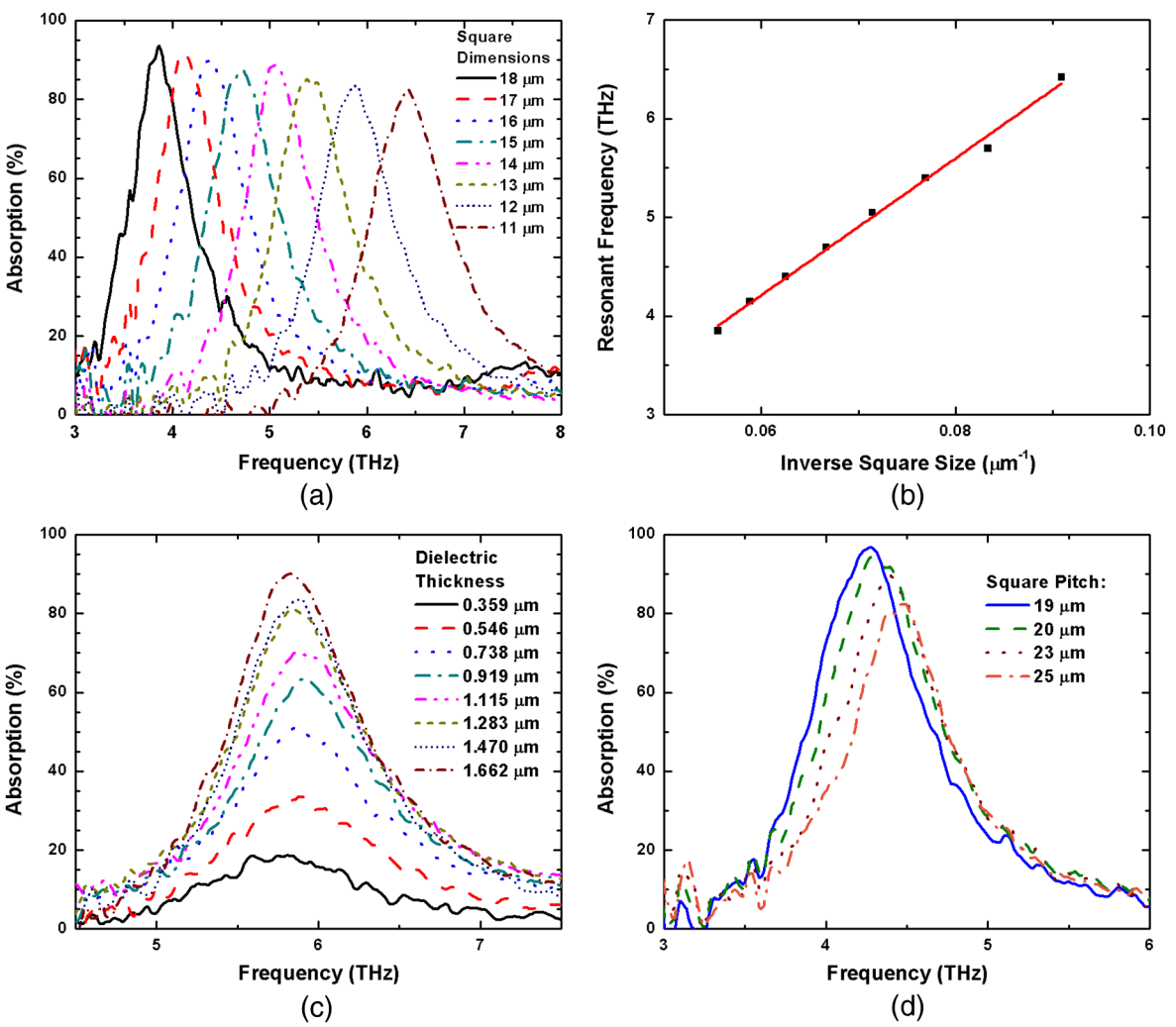

Fig. 5 FTIR measurements (a) for varying square size, 21 μm pitch, and 1.47 μm SiO$_x$. Linear fit (b) of inverse square size (1/s) to resonant absorption frequency (ν). The effects of varying dielectric thickness (c) for 12 μm squares and 21 μm pitch and varying pitch (d) with 16 μm squares and 1.47 μm SiO$_x$.

a relatively narrow spectral range. This behavior is ideal for applications requiring narrowband detection or involving pairing them with a narrow band source, such as a QCL for active THz imaging. However, in some cases, absorption in a broader spectral band is required, such as THz spectroscopy. Such metamaterial absorbers can be fabricated using more complex unit cells as described in the following section.

5 Metamaterials with Multiple Absorption Peaks

One approach to fabricating metamaterial absorbers with multiple absorption peaks is to introduce multiple resonators, for example, using squares of two different sizes. A possible configuration is to simply alternate the squares resulting in a pattern reminiscent of a checkerboard, as illustrated in Fig. 6(a) with squares dimensions of 13 and 17 μm and a dielectric layer thickness of 1.47 μm. Figure 6(c) shows the simulated absorption of structure in Fig. 6(a) along with absorption spectra by removing one type of squares and keeping the rest of the parameters the same. It can be easily seen from Fig. 6(c) that each type of square is responsible for one of the two peaks of the combined structure absorption. For the configuration shown in Fig. 6(a), the absorption measurement shows two well-separated absorption peaks at 4.25 and 5.5 THz [see Fig. 6(b)] similar to that obtained in the simulation. In addition, Fig. 6(b) shows measured single-band absorption from two complementary structures fabricated with only one type of square while maintaining the same dimension and pitch. In this case, single-absorption peaks clearly match with the absorption peaks of the dual-band absorber, indicating that each set of squares in Fig. 6(a) is responsible for generating the two peaks as predicted by the FE model [Fig. 6(c)]. As the difference in dimensions of square size is reduced (16 and 18 μm), the absorption peaks begin to overlap and merge together as illustrated by measured data in Fig. 6(d). Thus, by bringing the size of the squares closer together, it is possible to produce a broader absorption peak than a single square

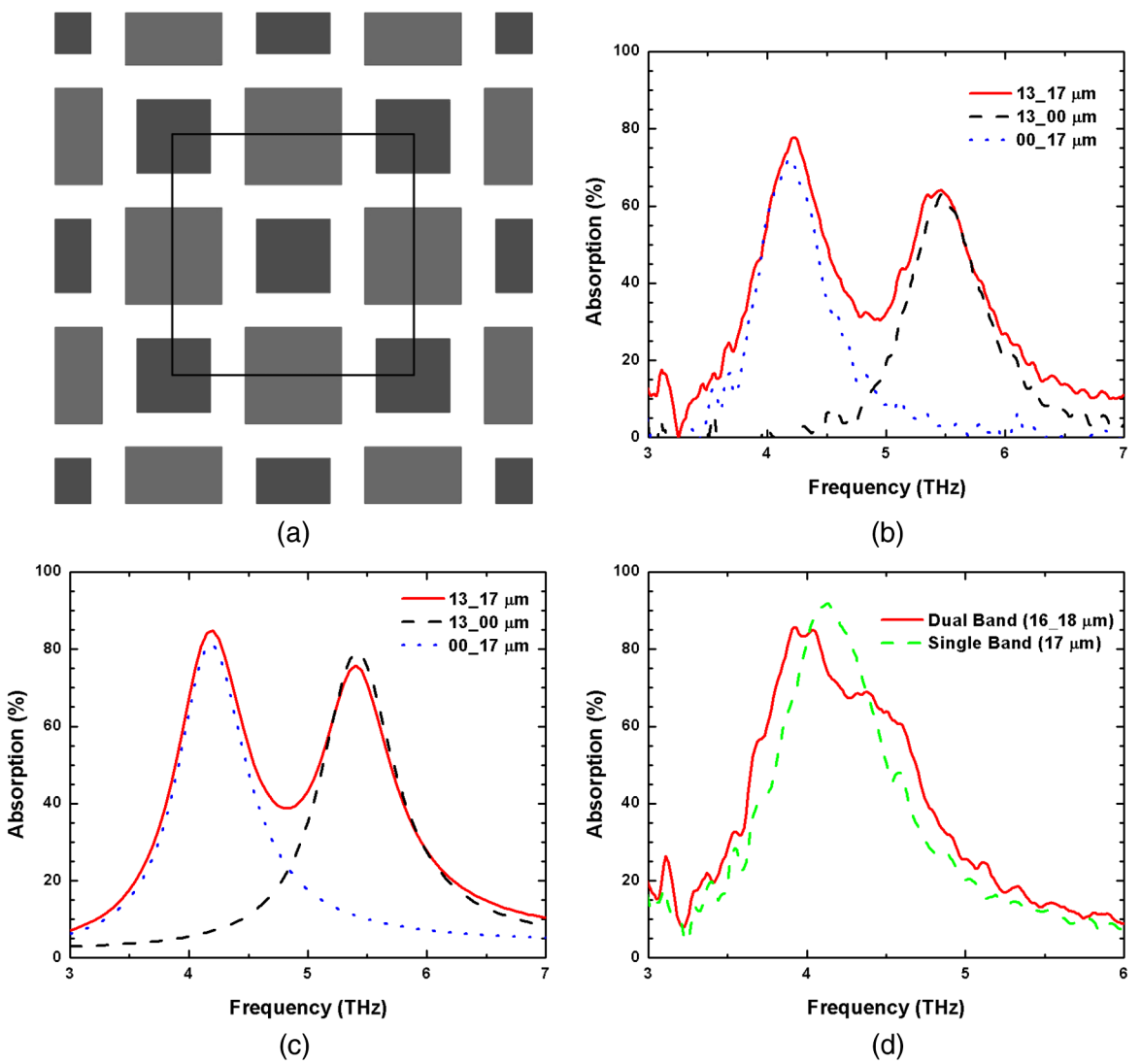

Fig. 6 Unit cell (a) of a dual band metamaterial configuration. Measured (b) and modeled (c) absorption for a dual band absorber with squares that have a 4 μm size difference compared to the same configuration with only one type of square. Comparison (d) of the absorption spectrum for dual band absorber with 2 μm square size difference, overall pitch of 42 μm and SiO$_x$ thickness 1.47 μm to a single band absorber with an intermediate square size.

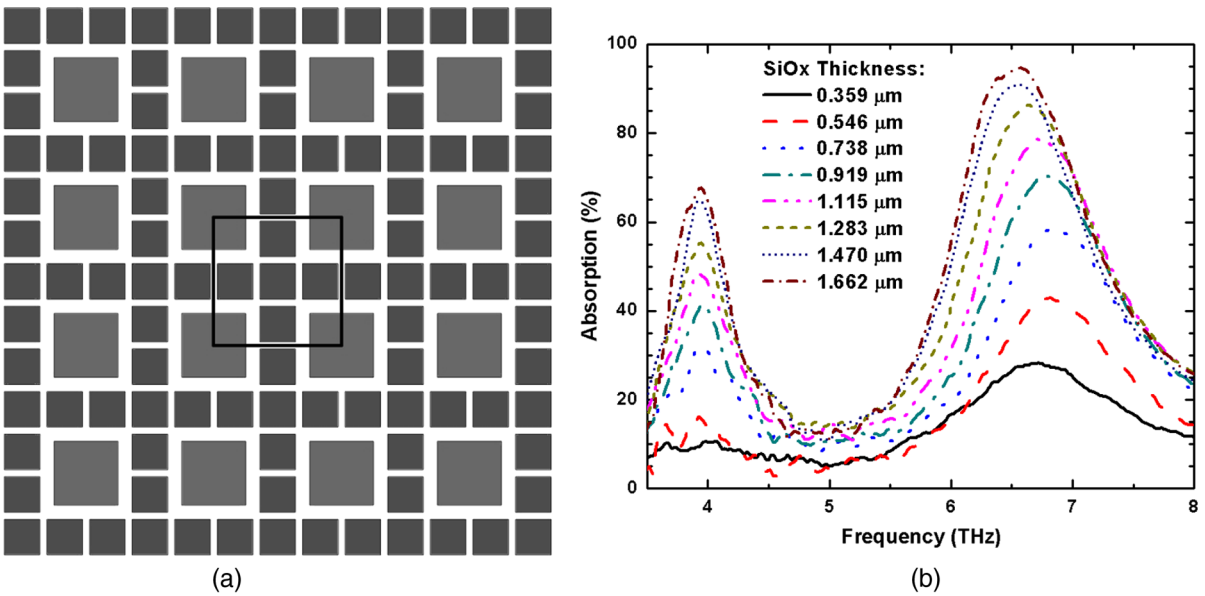

Fig. 7 Unit cell (a) and absorption characteristics (b) of a two peak metamaterial layer utilizing a tile configuration to maximize square density. (Use gray scale for the pattern.)

configuration of intermediate size (17 μm). In both the measurements and the FE model [Fig. 6(b) and 6(c)], it is apparent that the lower frequency absorption is enhanced while the higher frequency peak is suppressed. This causes the asymmetric peak shown in Fig. 6(d), as the two absorption peaks are merged by making the dimension of squares close to each other.

Another configuration for producing two absorption peaks is shown in Fig. 7(a) where smaller squares are placed around larger ones in a tile-like pattern. This configuration allows for squares with large size differences, and therefore absorption peaks at widely separated frequencies, to be more densely packed to increase absorption magnitude [as demonstrated in Fig. 5(b)]. Measurements showed two distinct absorption peaks at frequencies 4 and 6.5 THz, as depicted in Fig. 7(b), with the high frequency peak associated with the smaller square, as expected. Additionally, the higher frequency peak has a consistently larger magnitude, most likely due to the higher density of 10 μm squares. It is also apparent that the strength of the peak at 6.5 THz drops faster compared to the one at 4 THz as the thickness of the dielectric layer is increased. The 6.5 THz peak seems to be much more sensitive to changes in dielectric thickness compared to single-absorption peak configurations, such as Fig. 5(c).

The number of absorption peaks can be extended from dual-band absorbers by introducing additional square sizes. The geometry in Fig. 8(a) has three different squares (11, 14, and 17 μm) and maintains symmetry in two

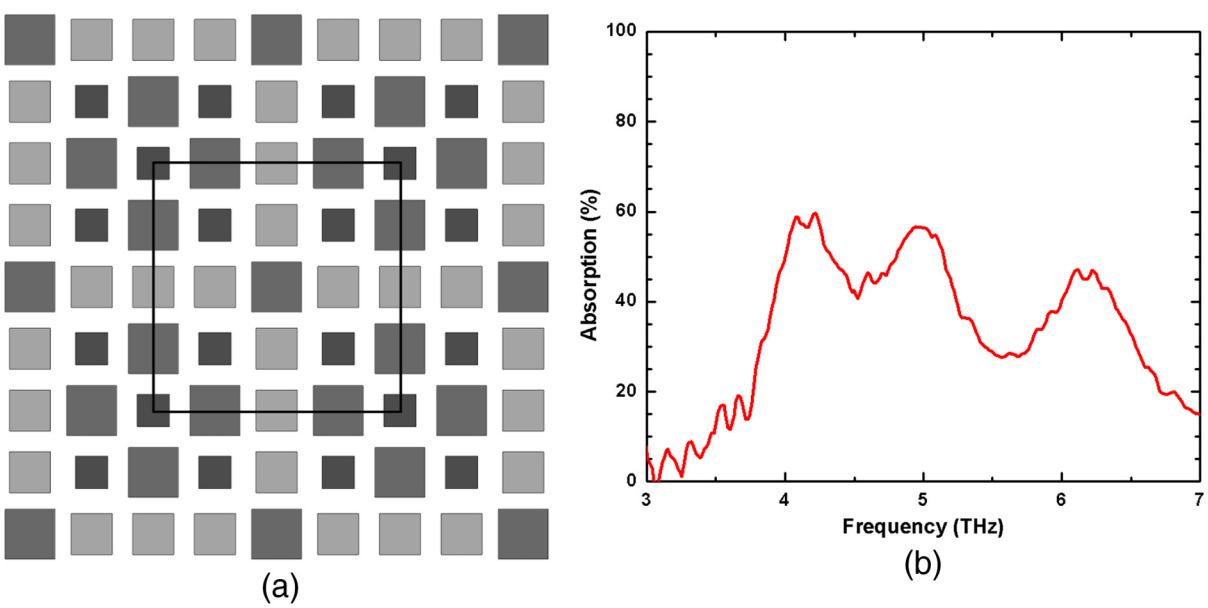

Fig. 8 Unit cell (a) and measured absorption (b) for a triple band metamaterial configuration with square sizes of 11, 14, and 17 μm showing three clear peaks.

directions, thus remaining polarization-independent at normal incidence, while also allowing for one of the squares (in this case the 14 μm squares) to have a 20% higher density, enhancing absorption at one of the corresponding resonant frequencies. This enhancement can be useful to increase absorption selectively if desired. As with the dual-band configuration, three distinct peaks associated with each square size can be resolved in the measured absorption spectrum in Fig. 8(b). In this case, the middle peak at 5 THz has a higher square density associated with it and an absorption peak of similar magnitude compared to the one corresponding to the larger squares at 4 THz. The overall absorption was found to be lower than that obtained for single-band and dual-band metamaterials.

6 Conclusion

We have demonstrated metamaterial THz absorbing layers with one, two, and three absorption peaks that are less than 2 μm thick using Al for the metal layers and Si-rich low-stress SiO_x as a dielectric spacer. Al and SiO_x are standard microfabrication materials, and can therefore be easily incorporated into the construction of thermal sensors such as microbolometers or bi-material sensors.[31] If these layers are used in a microbolometer pixel, the thickness of the microbridge could be minimized by placing the resistive layer in the dielectric spacer. Further investigation is needed to determine what impact this will have on absorption. These metamaterial structures demonstrate tunable resonant absorption through modifications to their geometry. Resonant absorption frequency is controlled through adjustments to the size of the square patches. By controlling dielectric thickness and square pitch it is possible to achieve nearly 100% absorption with only minor changes to the resonant absorption frequency (compensated by adjusting square size). Additionally, multiple or broadened absorption peaks can be produced through the introduction of multiple square sizes. The results indicate that these metamaterial absorbers can be used as absorbing layers in thermal imagers paired with narrow band sources to significantly enhance their sensitivity through resonant absorption at the emitter frequency. In addition, dual- and triple-band configurations can be used with multiple lasers or broader sources, as desired.

Acknowledgments

This work is supported, in part, through a grant from the Oak Ridge National Laboratory (ONR). The authors would like to thank Raymond Ng, Nick Lavrik, Jay Adeff, and Sam Barone for technical assistance. A portion of this research was conducted at the Center for Nanophase Materials Sciences, which is sponsored at ORN Laboratory by the Office of Basic Energy Sciences, U.S. Department of Energy.

References

1. J. F. Federici et al., "THz imaging and sensing for security applications–explosives, weapons, and drugs," *Semicond. Sci. Technol.* **20**(7), S266–S280 (2005).
2. S. M. Kim et al., "Biomedical terahertz imaging with a quantum cascade laser," *Appl. Phys. Lett.* **88**(15), 153903 (2006).
3. Z. D. Taylor et al., "Reflective terahertz imaging of porcine skin burns," *Opt. Lett.* **33**(11), 1258–1260 (2008).
4. J. E. Bjarnason et al., "Millimeter-wave, terahertz, and midinfrared transmission through common clothing," *Appl. Phys. Lett.* **85**(4), 519 (2004).
5. R. H. Clothier and N. Bourne, "Effects of THz exposure on human primary keratinocyte differentiation and viability," *J. Biol. Phys.* **29**(2–3), 179–85 (2003).
6. A. W. M. Lee and Q. Hu, "Real-time, continuous-wave terahertz imaging by use of a microbolometer focal-plane array," *Opt. Lett.* **30**(19), 2563–2565 (2005).
7. A. W. M. Lee et al., "Real-time imaging using a 4.3-THz quantum cascade laser and a 320 × 240 microbolometer focal-plane array," *IEEE Photon. Technol. Lett.* **18**(13), 1415 (2006).
8. B. N. Behnken et al., "Detection of 3.4 THz radiation from a quantum cascade laser using a microbolometer infrared camera," *Proc. SPIE* **6549**, 65490C (2007).
9. M. J. Coppinger, "Sensitivity of a vanadium oxide uncooled microbolometer array for terahertz imaging," *Opt. Eng.* **50**(5), 053206 (2011).
10. H. Budzier and G. Gerlach, *Thermal Infrared Sensors: Theory, Optimization and Practice*, pp. 226–227, Wiley, West Sussex (2011).
11. C. M. Watts, X. Liu, and W. J. Padilla, "Metamaterial electromagnetic wave absorbers," *Adv. Mater.* **24**(23), OP98–OP120 (2012).
12. F. Alves et al., "Strong terahertz absorption using SiO_2/Al based metamaterial structures," *Appl. Phys. Lett.* **100**(11), 111104 (2012).
13. F. Alves et al., "MEMS bi-material terahertz sensor with integrated metamaterial absorber," *Opt. Lett.* **37**(11), 1886–1888 (2012).
14. T. Maier and H. Bruckl, "Wavelength-tunable microbolometers with metamaterial absorbers," *Opt. Lett.* **34**(19), 3012–3014 (2009).
15. H. Tao et al., "Microwave and terahertz wave sensing with metamaterials," *Opt. Express* **19**(22), 21620–21626 (2011).
16. Y. Todorov et al., "Optical properties of metal-dielectric-metal microcavities in the THz frequency range," *Opt. Express* **18**(13), 13886 (2010).
17. L. Huang and H. Chen, "Multi-band and polarization insensitive metamaterial absorber," *PIER* **113**, 103–110 (2011).
18. X. Shen et al., "Polarization-independent wide-angle triple-band metamaterial absorber," *Opt. Express.* **19**(10), 9401 (2011).
19. H. Li et al., "Ultrathin multiband gigahertz metamaterial absorbers," *J. Appl. Phys.* **110**(1), 014909 (2011).
20. Q.-Y. Wen et al., "Dual band terahertz metamaterial absorber: design, fabrication, and characterization," *Appl. Phys. Lett.* **95**(24), 241111 (2009).
21. L. Huang et al., "Experimental demonstration of terahertz metamaterial absorbers with a broad and flat absorption band," *Opt. Lett.* **37**(2), 154–156 (2012).
22. H. Tao et al., "A dual band terahertz metamaterial absorber," *J. Phys. D: Appl. Phys.* **43**(22), 225102 (2010).
23. X.-J. He et al., "Dual-band terahertz metamaterial absorber with polarization insensitivity and wide incident angle," *PIER* **115**, 381–397 (2011).
24. Y. Ma et al., "A terahertz polarization insensitive dual band metamaterial absorber," *Opt. Lett.* **36**(6), 945–947 (2011).
25. B. Zhang et al., "Polarization-independent dual-band infrared perfect absorber based on a metal-dielectric-metal elliptical nanodisk array," *Opt. Express* **19**(16), 15221 (2011).
26. X. Liu et al., "Taming the blackbody with infrared metamaterials as selective thermal emitters," *Phys. Rev. Lett.* **107**(4), 045901 (2011).
27. N. I. Landy et al., "Perfect metamaterial absorber," *Phys. Rev. Lett.* **100**(20), 207402 (2008).
28. H.-T. Chen, "Interference theory of metamaterial perfect absorbers," *Opt. Express* **20**(7), 7165–7172 (2012).
29. Q.-Y Wen et al., "Transmission line model and fields analysis of metamaterial absorber in the terahertz band," *Opt. Express* **17**(22), 20256–20265 (2009).
30. D. Y. Smith et al., Eds., *Handbook of Optical Constants of Solids*, Academic Press, San Diego & Chesnut Hill (1998).
31. P. G. Datskos et al., "Infrared imaging using arrays of SiO_2 micromechanical detectors," *Opt. Lett.* **37**(19) 171066 (2012).

Brian Kearney received his BA in astrophysics and physics from the University of California at Berkeley in 2008. He is currently a PhD candidate at the Physics Department of the Naval Postgraduate School working under Professor Gamani Karunasiri. His research interests include integration of THz absorbing films into thermal sensors, particularly micro-bolometer membranes to improve real time THz imaging performance.

Fabio Alves received his PhD in physics in 2008 from the Instituto Tecnologico de Aeronautica, Brazil, where he is currently a collaborating professor, in addition to a National Research Council research associate in the Physics Department of the Naval Postgraduate School. He has researched infrared detectors, micro-electro-mechanical systems (MEMS) sensors and Aircraft IR signatures and currently works on metamaterial absorbers, thin films, and real-time THz imaging using bi-material sensor arrays.

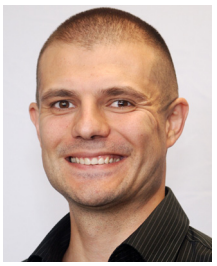

Dragoslav Grbovic received a BS in physics from Ramapo College of New Jersey in 2003 and a PhD in physics from the University of Tennessee in 2008. He is currently an assistant professor at the Physics Department of the Naval Postgraduate School. His research interests include micro-electro-mechanical systems (MEMS) for sensing and energy-harvesting applications, with recent research focusing on creating focal plane arrays of bi-material MEMS devices for infrared and terahertz imaging. He has extensive experience in MEMS device design and simulation, as well as photolithography and micro-fabrication processes.

Gamani Karunasiri received his PhD from the University of Pittsburgh in 1984 and joined the faculty of the Physics Department of the Naval Postgraduate School in 2000. He conducts research in multicolor infrared detectors, uncooled infrared and THz sensors and semiconductor sensors that mimic biological vision and auditory systems. He has published more than 100 journal papers, held the Andrew Mellon Predoctoral Fellowship from the University of Pittsburgh and won teaching honors and awards from the National University of Singapore.